usual diffraction spots, diffraction discs (in Laue or transmission geometry) were produced. The diffraction intensity within a disc shows a specific symmetry, which enables one to determine the point groups and space groups of microcrystals. Unlike X-ray diffraction, the method is extremely sensitive to the presence or absence of inversion symmetry.

The method corresponding to CBED in the field of light optics is the conoscope method. Using a conoscope, we can identify whether a crystal is isotropic, uniaxial or biaxial, and determine the optic axis and the sign of birefringence of a crystal. When CBED, a conoscope method using an electron beam, is utilized, more basic properties of a crystal – the crystal point group and space group – can be determined.

Point- and space-group determinations are routinely also carried out by X-ray diffraction. This method, to which kinematical diffraction is applicable, cannot determine whether a crystal is polar or nonpolar unless anomalous absorption is utilized. As a result, the X-ray diffraction method can only identify 11 Laue groups among 32 point groups. CBED, based fully upon dynamical diffraction, can distinguish polar crystals from nonpolar crystals using only a nanometre-sized crystal, thus allowing the unique identification of all the point groups by inspecting the symmetries appearing in CBED discs.

As pointed out above, an unambiguous experimental determination of crystal symmetry, in the case of X-ray diffraction, is usually not possible because of the apparent centrosymmetry of the diffraction pattern, even for noncentrosymmetric crystals. However, methods based on structure-factor and X-ray intensity statistics remain useful for the resolution of space-group ambiguities, and are routinely applied to structure determinations from X-ray data. These methods are described in Chapter 2.1 of this volume.

In the field of materials science, correct space-group determination by CBED is often requested prior to X-ray or neutron structure refinement, in particular in the case of Rietveld refinements based on powder diffraction data.

CBED can determine not only the point and space groups of crystals but also crystal structure parameters – lattice parameters, atom positions, Debye–Waller factors and low-order structure factors. The lattice parameters can be determined from submicron regions of thin crystals by using higher-order Laue zone (HOLZ) reflections with an accuracy of 1×10^{-4}. Cherns *et al.* (1988) were the first to perform strain analysis of artificial multilayer materials using the large-angle technique (LACBED) (Tanaka *et al.*, 1980). Since then, many strain measurements at interfaces of various multilayer materials have been successfully conducted. In recent years, strain analysis has been conducted using automatic analysis programs, which take account of dynamical diffraction effects (Krämer *et al.*, 2000). We refer to the book of Morniroli (2002), which carries many helpful figures, clear photographs and a comprehensive list of papers on this topic.

Vincent *et al.* (1984*a*,*b*) first applied the CBED method to the determination of the atom positions of AuGeAs. They analysed the intensities of HOLZ reflections by applying a quasi-kinematical approximation. Tanaka & Tsuda (1990, 1991) and Tsuda & Tanaka (1995) refined the structural parameters of $SrTiO_3$ by applying the dynamical theory of electron diffraction. The method was extended to the refinements of CdS, $LaCrO_3$ and hexagonal $BaTiO_3$ (Tsuda & Tanaka, 1999; Tsuda *et al.*, 2002; Ogata *et al.*, 2004). Rossouw *et al.* (1996) measured the order parameters of TiAl through a Bloch-wave analysis of HOLZ reflections in a CBED pattern. Midgley *et al.* (1996) refined two positional parameters of $AuSn_4$ from the diffraction data obtained with a small convergence angle using multislice calculations.

Low-order structure factors were first determined by Goodman & Lehmpfuhl (1967) for MgO. After much work on low-order structure-factor determination, Zuo & Spence determined the 200 and 400 structure factors of MgO in a very modern way, by fitting energy-filtered patterns and many-beam dynamical calculations using a least-squares procedure. For the low-order structure-factor determinations, the excellent comprehensive review of Spence (1993) should be referred to. Saunders *et al.* (1995) succeeded in obtaining the deformation charge density of Si using the low-order crystal structure factors determined by CBED. For the reliable determination of the low-order X-ray crystal structure factors or the charge density of a crystal, accurate determination of the Debye–Waller factors is indispensable. Zuo *et al.* (1999) determined the bond-charge distribution in cuprite. Simultaneous determination of the Debye–Waller factors and the low-order structure factors using HOLZ and zeroth-order Laue zone (ZOLZ) reflections was performed to determine the deformation charge density of $LaCrO_3$ accurately (Tsuda *et al.*, 2002).

CBED can also be applied to the determination of lattice defects, dislocations (Cherns & Preston, 1986), stacking faults (Tanaka, 1986) and twins (Tanaka, 1986). Since this topic is beyond the scope of the present chapter, readers are referred to pages 156 to 205 of the book by Tanaka *et al.* (1994).

We also mention the book by Spence & Zuo (1992), which deals with the whole topic of CBED, including the basic theory and a wealth of literature.

2.5.3.2. Point-group determination

When an electron beam traverses a thin slab of crystal parallel to a zone axis, one can easily imagine that symmetries parallel to the zone axis should appear in the resulting CBED pattern. It is, however, more difficult to imagine what symmetries appear due to symmetries perpendicular to the incident beam. Goodman (1975) pioneered the clarification of CBED symmetries for the twofold rotation axis and mirror plane perpendicular to the incident beam, and the symmetry of an inversion centre, with the help of the reciprocity theorem of scattering theory. Tinnappel (1975) solved many CBED symmetries at various crystal settings with respect to the incident beam using a group-theoretical treatment. Buxton *et al.* (1976) also derived these results from first principles, and generalized them to produce a systematic method for the determination of the crystal point group. Tanaka, Saito & Sekii (1983) developed a method to determine the point group using simultaneously excited many-beam patterns. The point-group-determination method given by Buxton *et al.* (1976) is described with the aid of the description by Tanaka, Saito & Sekii (1983) in the following.

2.5.3.2.1. Symmetry elements of a specimen and diffraction groups

Since CBED uses the Laue geometry, Buxton *et al.* (1976) assumed a perfectly crystalline specimen in the form of a parallel-sided slab which is infinite in two dimensions. The symmetry elements of the *specimen* (as distinct from those of an infinite crystal) form 'diffraction groups', which are isomorphic to the point groups of the diperiodic plane figures and Shubnikov groups of coloured plane figures. The diffraction groups of a specimen are determined from the symmetries of CBED patterns taken at various orientations of the specimen. The *crystal* point-group of the specimen is identified by referring to Fig. 2.5.3.4, which gives the relation between diffraction groups and crystal point groups.

A specimen that is parallel-sided and is infinitely extended in the x and y directions has ten symmetry elements. The symmetry elements consist of six two-dimensional symmetry elements and four three-dimensional ones. The operation of the former elements transforms an arbitrary coordinate (x, y, z) into (x', y', z), with z remaining the same. The operation of the latter transforms a coordinate (x, y, z) into (x', y', z'), where $z' \neq z$. A vertical mirror plane m and one-, two-, three-, four- and sixfold rotation axes that are parallel to the surface normal **z** are the two-

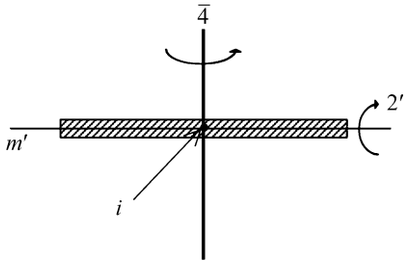

Fig. 2.5.3.1. Four symmetry elements m', i, $2'$ and $\bar{4}$ of an infinitely extended parallel-sided specimen.

Table 2.5.3.1. *Two- and three-dimensional symmetry elements of an infinitely extended parallel-sided specimen*

Symbols in parentheses show CBED symmetries appearing in dark-field patterns.

Two-dimensional symmetry elements	Three-dimensional symmetry elements
1	m' (1_R)
2	i (2_R)
3	$2'$ (m_2, m_R)
4	$\bar{4}$ (4_R)
5	
6	
m	

dimensional symmetry elements. A horizontal mirror plane m', an inversion centre i, a horizontal twofold rotation axis $2'$ and a fourfold rotary inversion $\bar{4}$ are the three-dimensional symmetry elements, and are shown in Fig. 2.5.3.1. The fourfold rotary inversion was not recognized as a symmetry element until the point groups of the diperiodic plane figures were considered (Buxton *et al*., 1976). Table 2.5.3.1 lists these symmetry elements, where the symbols in parentheses express symmetries of CBED patterns expected from three-dimensional symmetry elements.

The diffraction groups are constructed by combining these symmetry elements (Table 2.5.3.2). Two-dimensional symmetry elements and their combinations are given in the top row of the table. The third symmetry m in parentheses is introduced automatically when the first two symmetry elements are combined. Three-dimensional symmetry elements are given in the first column. The equations given below the table indicate that no additional three-dimensional symmetry elements can appear by combination of two symmetry elements in the first column. As a result, 31 diffraction groups are produced by combining the elements in the first column with those in the top row. Diffraction groups in square brackets have already appeared ealier in the table. In the fourth row, three columns have two diffraction groups, which are produced when symmetry elements are combined at different orientations. In the last row, five columns are empty because a fourfold rotary inversion cannot coexist with threefold and sixfold rotation axes. In the last column, the number of independent diffraction groups in each row is given, the sum of the numbers being 31.

2.5.3.2.2. Identification of three-dimensional symmetry elements

It is difficult to imagine the symmetries in CBED patterns generated by the three-dimensional symmetry elements of the sample. The reason is that if a three-dimensional symmetry element is applied to a specimen, it turns it upside down, which is impractical in most experiments. The reciprocity theorem of scattering theory (Pogany & Turner, 1968) enables us to clarify the symmetries of CBED patterns expected from these three-dimensional symmetry elements. A graphical method for obtaining CBED symmetries due to sample symmetry elements is described in the papers of Goodman (1975), Buxton *et al*. (1976) and Tanaka (1989). The CBED symmetries of the three-dimensional symmetries do not appear in the zone-axis patterns, but do in a diffraction disc set at the Bragg condition, each of which we call a dark-field pattern (DP). The CBED symmetries obtained are illustrated in Fig. 2.5.3.2. A horizontal twofold rotation axis $2'$, a horizontal mirror plane m', an inversion centre i and a fourfold rotary inversion $\bar{4}$ produce symmetries m_R (m_2), 1_R, 2_R and 4_R in DPs, respectively.

Next we explain the symbols of the CBED symmetries. (1) Operation m_R is shown in the left-hand part of Fig. 2.5.3.2(*a*), which implies successive operations of (*a*) a mirror m with respect to a twofold rotation axis, transforming an open circle beam (○) in reflection G into a beam (+) in reflection G' and (*b*) rotation R of this beam by π about the centre point of disc G' (or the exact Bragg position of reflection G'), resulting in position ○ in reflection G'. The combination of the two operations is written as m_R. When the twofold rotation axis is parallel to the diffraction vector **G**, two beams (○) in the left-hand part of the figure become one reflection G, and a mirror symmetry, whose mirror line is perpendicular to vector **G** and passes through the centre of disc G, appears between the two beams (the right-hand side figure of Fig. 2.5.3.2*a*). The mirror symmetry is labelled m_2 after the twofold rotation axis. (2) Operation 1_R (Fig. 2.5.3.2*b*) for a horizontal mirror plane is a combination of a rotation by 2π of a beam (○) about a zone axis O (symbol 1), which is equivalent to no rotation, and a rotation by π of the beam about the exact Bragg position or the centre of disc G. (3) Operation 2_R is a rotation by π of a beam (○) in reflection G about a zone axis (symbol 2), which transforms the beam into a beam (+) in reflection $-G$, followed by a rotation by π of the beam (+) about the centre of disc $-G$, resulting in the beam (○) in disc $-G$ (Fig. 2.5.3.2*c*). The symmetry is called translational symmetry after Goodman (1975) because the pattern of disc $+G$ coincides with that of disc $-G$ by a translation. It is emphasized that an inversion centre is identified by the test of translational symmetry about a pair of $\pm G$ dark-field patterns – if one disc can be translated into coincidence with the other, an inversion centre exists. We call the pair ±DP. (4) Operation 4_R (Fig. 2.5.3.2*d*) can be understood in a similar manner. It is noted that regular letters are symmetries about a zone axis, while subscripts R represent symmetries about the exact Bragg position. We call a pattern that contains an exact Bragg position (if possible at the disc centre) a dark-field pattern. As far as CBED symmetries are concerned, we

Table 2.5.3.2. *Symmetry elements of an infinitely extended parallel-sided specimen and diffraction groups*

	1	2	3	4	6	m	$2m(m)$	$3m$	$4m(m)$	$6m(m)$	
1	1	2	3	4	6	m	$2m(m)$	$3m$	$4m(m)$	$6m(m)$	10
(m') 1_R	1_R	21_R	31_R	41_R	61_R	$m1_R$	$2m(m)1_R$	$3m1_R$	$4m(m)1_R$	$6m(m)1_R$	10
(i) 2_R	2_R	$[21_R]$	6_R	$[41_R]$	$[61_R]$	$2_Rm(m_R)$	$[2m(m)1_R]$	$6_Rm(m_R)$	$[4m(m)1_R]$	$[6m(m)1_R]$	4
						$[2_Rm(m_R)]$	$[2m(m)1_R]$	$[3m1_R]$			
($2'$) m_R	m_R	$2m_R(m_R)$	$3m_R$	$4m_R(m_R)$	$6m_R(m_R)$	$[m1_R]$	$[4_R(m)m_R]$	$[6_Rm(m_R)]$	$[4m(m)1_R]$	$[6_Rm(m_R)]$	5
($\bar{4}$) 4_R		4_R		$[41_R]$		$4_Rm(m_R)$	$[4_Rm(m_R)]$		$[4m(m)1_R]$		2

$1_R \times 2_R = 2$, $2_R \times 2_R = 1$, $m_R \times 2_R = m$, $4_R \times 2_R = 4$, $1_R \times m_R = m \times m_R$, $1_R \times 4_R = 4 \times 1_R$, $m_R \times 4_R = m \times 4_R$.